Ligia R. Gomes, John N. Low*, Tanja van Mourik, Ligia S. da Silveira Pinto,
Marcus V.N. de Souza and Jámes L. Wardell*

Crystal structures, Hirsfeld surface analysis and a computational study of four ethyl 2-oxo-2*H*-chromene-3-carboxylate derivatives: a survey of organyl 2-oxo-2*H*-chromene-3-carboxylate structures

Abstract: Crystal structures, Hirshfeld surface analysis and a computational study have been carried out on 2-oxo-2*H*-chromene-3-carboxylates. Crystal structures are reported for ethyl R-2-oxo-2*H*-chromene-3-carboxylate derivatives, **2a:** R = 6-Me, **2b:** 7-Me, **2c:** 7-Me, **2d:** R = 7-MeO. In contrast to 2-oxo-2H-chromene-3-carboxamides, **1**, in which classical intramolecular N−H···O hydrogen bonds stabilize planar structures and hinder rotation of the amido group out of the coumarin plane in **2**, without an equivalent hydrogen bond, there is a greater rotational freedom of the carboxylate group. The interplanar angles between the coumarin core and its attached −C(O)−R substituent in crystalline **2a**, **2b**, **2c** and **2d** are 10.41(6), 36.65(6), 10.4(2) and 5.64(6)°, respectively, with distances between the carbonyl oxygen atoms of 2.8255(16), 2.9278(16), 4.226(2) and 2.8328(14) Å, respectively. A theoretical study of molecular conformations was carried out at the M06-2X density level with the 6-31+G(d) and aug-cc-pVTZ basis sets, in methanol solution modeled by PCM, indicated that the most stable conformations had the carbonyl group of the ester in the plane of the coumarin core: the *s-cis* arrangement of the ester carbonyl and the 2-oxo moieties being the slightly more stable than the *s-trans* form by less than 0.5 kcal/mol. The experimental conformations of **2a** and **2d** match well the low energy *s-cis* arrangement, and **2c** matches the slightly lesser stable *s-trans* arrangement found in the theoretical study. A survey of the molecular conformations of more than 50 2*H*-chromene-3-carboxylates derivatives in the CCDC data base indicated two distinct groupings of conformations, *s-cis* and *s-trans*, each with interplanar angles <30°.

Keywords: 2-oxo-2*H*-chromene-3-carboxylate derivatives; crystal structures; density functional theory; Hirshfeld surface analysis; molecular conformation.

*Corresponding authors: John N. Low, Department of Chemistry, University of Aberdeen, Meston Walk, Old Aberdeen, AB24 3UE, Scotland, UK, E-mail: jnlow111@gmail.com; and **Jámes L. Wardell,** Department of Chemistry, University of Aberdeen, Meston Walk, Old Aberdeen, AB24 3UE, Scotland, UK; and Instituto de Tecnologia em Fármacos e Farmanguinhos, Fundação Oswaldo Cruz, 21041-250 Rio de Janeiro, RJ, Brazil, E-mail: j.wardell@abdn.ac.uk
Ligia R. Gomes: FP-ENAS-Faculdade de Ciências de Saúde, Escola Superior de Saúde da UFP, Universidade Fernando Pessoa, Rua Carlos da Maia, 296, P-4200-150 Porto, Portugal; and REQUIMTE, Departamento de Química e Bioquímica, Faculdade de Ciências da Universidade do Porto, Rua do Campo Alegre, 687, P-4169-007, Porto, Portugal
Tanja van Mourik: School of Chemistry, University of St. Andrews, North Haugh, St. Andrews, Fife KY16 9ST, Scotland, UK
Ligia S. da Silveira Pinto: Universidade Federal do Rio de Janeiro, Instituto de Química, Departamento de Química Orgânica, CP 68563, 21945-970, Rio de Janeiro, Brazil; and Instituto de Tecnologia em Fármacos e Farmanguinhos, Fundação Oswaldo Cruz, 21041-250 Rio de Janeiro, RJ, Brazil
Marcus V.N. de Souza: Instituto de Tecnologia em Fármacos e Farmanguinhos, Fundação Oswaldo Cruz, 21041-250 Rio de Janeiro, RJ, Brazil

Introduction

2*H*-Chromene-2-ones, or coumarins, are a group of natural product found in many plant species belonging to the benzopyrone family. Derivatives, both natural and man-made, have been found to have a wide range of pharmacological activities [1–3], including as anti-HIV [4, 5], antibacterial [6, 7], antifungal [8], anti-inflammatoryl [9], anti-TB [10, 11], antileishmanial [12], antimalarial [13], antitumor [14–16], and antidepressant activities [17], and act as anticoagulants [18], α-glucosidase inhibitors [19], topoisomerase II inhibitors [20], cholinesterase inhibitors [21], Alzheimer's diseaseinhibitors [22], and antioxidants [23, 24]. Coumarins also have applications in cosmetics and can be used as optical brightening agents, laser dyes, and fluorescence markers [25, 26] and as liquid crystals [27].

The synthesis of the 2*H*-chromene-2-ones nucleus was first described in 1868 [28]. Since then, in keeping with their utilities, various synthetic procedures have been devised [29, 30]. The interest in establishing new synthetic routes continues today [31–33]. Among the recent developments has been the use of ultrasonics in the reactions between active methylene compounds and 2-hydroxybenzaldehydes or resorcinol [34].
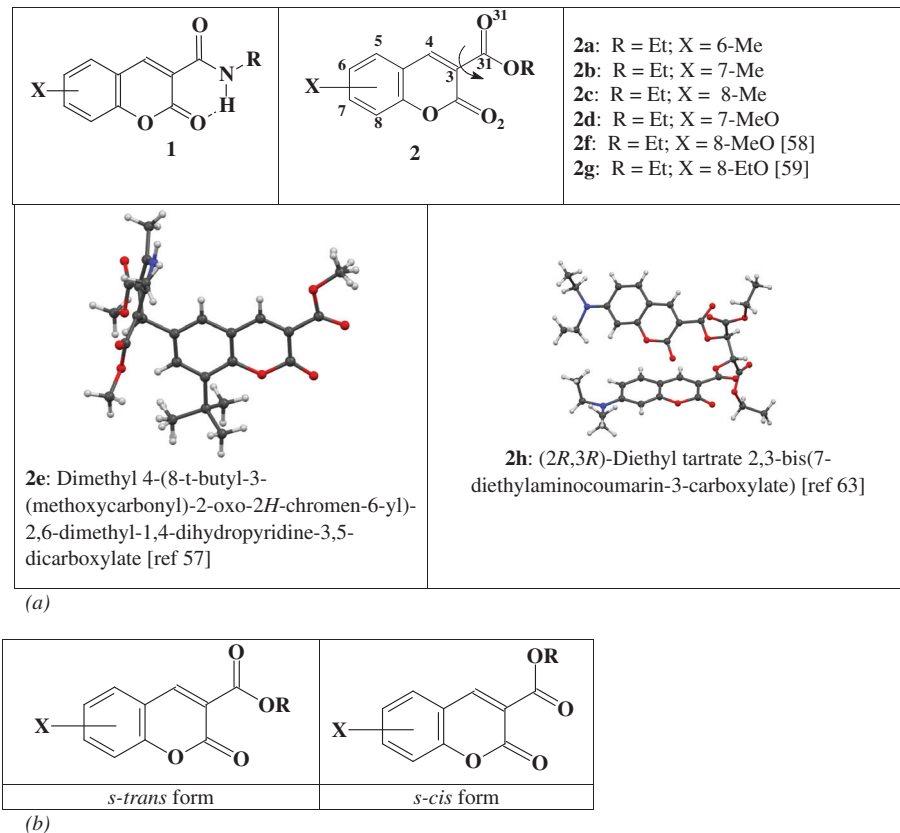
As part of our ongoing structural studies of compounds having biological activities [35–38], some of us have reported the structures of 2-oxo-2*H*-chromene-3-carboxamides, **1**, see Figure 1 [39, 40]. These studies, and a survey of related compounds in the CCDC data base, indicated the near planarity of such molecules arising from the very strong classical intramolecular N–H···O hydrogen bond, involving the amido group and the chromene carbonyl oxygen atom, which essentially fixes the overall conformation to be near planar, see Figure 1. Alkyl 2-oxo-2*H*-chromene-3-carboxylates, **2**, see Figure 1, do not possess the ability to form a strong intramolecular hydrogen bond from the carboxylate and oxo group. Without a strong stabilizing hydrogen bond, compounds **2** will have the freedom to rotate about the coumarin-carboxylate bond and thus have potential for a range of differing conformations.

With ready access to alkyl 2-oxo-2*H*-chromene-3-carboxylates, prepared using ultrasonics [34], we initiated a crystal structural and Hirshfeld surface study of such carboxylates. Four compounds were chosen, for study, namely 3-ethoxycarbonyl-6-methylcoumarin, **2a**, 3-ethoxycarbonyl-7-methylcoumarin, **2b**, 3-ethoxycarbonyl-8-methylcoumarin, **2c** and 3-ethoxycarbonyl-7-methoxycoumarin, **2d**, see Figure 1. Each of the chosen compounds has relatively small substituents in order to avoid the influence of serious steric effects on the structures. The structures were solved from data collected at 100 K. The crystal structure of **2d** had been previously determined from data collected at 296 K (Ref. [41]: CCDC. KIWCIE: 928907): the same phase was obtained at both temperatures.

The molecular conformation is the basic building block for developing the crystal structure and thus is an important feature to investigate. However, due to the possibility of bond rotation in solution, the solid state conformation may be greatly changed on dissolution. To see what changes may occur in a model solvent, a computational study of the molecular conformations of the compounds was carried out at the M06-2X density level with the 6-31+G(d) and aug-cc-pTVZ basis sets, in methanol solution modelled by the Polarizable Continuum Model.

Comparisons of the structural features found in this study were made with those of organyl 2*H*-chromene-3-carboxylate compounds present in the CCDC data on Jun 22nd, 2017.

2a: R = Et; X = 6-Me
2b: R = Et; X = 7-Me
2c: R = Et; X = 8-Me
2d: R = Et; X = 7-MeO
2f: R = Et; X = 8-MeO [58]
2g: R = Et; X = 8-EtO [59]

2e: Dimethyl 4-(8-t-butyl-3-(methoxycarbonyl)-2-oxo-2*H*-chromen-6-yl)-2,6-dimethyl-1,4-dihydropyridine-3,5-dicarboxylate [ref 57]

2h: (2*R*,3*R*)-Diethyl tartrate 2,3-bis(7-diethylaminocoumarin-3-carboxylate) [ref 63]

(a)

s-trans form   *s-cis* form

(b)

Fig. 1: (a) Compounds dealt with in this study, (b) *cis* and *trans* forms of **2**.

Experimental

General synthesis

The compounds were produced as previously reported, see Scheme 1 [34]. The samples used in the crystal structure determinations were grown from methanol solutions. Physical properties were in agreement with reported values [34].

Experimental crystallography

Details of the data collection and refinement are given in Table 1 [42–47].

The Hirshfeld surface analysis

The Hirshfeld surfaces and two-dimensional fingerprint (FP) plots [48] were generated using Crystal Explorer 3.1 [49]. The Hirshfeld surfaces were mapped over d_{norm} (all scaled between −0.250 and 1.200). The Hirshfeld surfaces and FP plots for the four compounds are discussed at appropriate points in the Results and Discussion section.

Computational methodology

Starting structures for geometry optimizations were created from the X-ray crystal structures of the different coumarins, with further geometries formed by rotating around the flexible bonds. Dihedral angles of 0 and 180° were used for the rotation of the $_{(coumarin)}C–O_{(OEt)}$ bond in all four molecules and for the $O–CH_3$ bond in **2d**, and values of 0, 90, 180 and 270° for the last two bonds in the $O=C–O–CH_2–CH_3$ moiety. The structures were optimized using the M06-2X density functional [50] and the 6-31+G(d) basis set, in methanol solution modelled by the Polarizable Continuum Model [51] using the integral equation formalism variant (IEFPCM). The optimized structures were sorted into different groups (A–G) and selected conformers were re-optimized at the M06-2X/aug-cc-pVTZ level [52, 53]. All calculations were carried out with Gaussian 09 [54] and employed Gaussian's "ultrafine" integration

Tab. 1: Crystallographic details.

	2a	2b	2c	2d
Crystal data				
Chemical formula	$C_{13}H_{12}O_4$	$C_{13}H_{12}O_4$	$C_{13}H_{12}O_5$	$C_{13}H_{12}O_4$
M_r	232.23	232.23	248.23	232.23
Crystal system, space group	*Monoclinic*, *C2/c*	*Monoclinic*, *P2₁/c*	*Monoclinic*, *C2/c*	*Monoclinic*, *C2/c*
Temperature (K)	100	100	100	100
a, b, c (Å)	23.8307 (5), 7.1205 (2), 13.4435 (8)	13.1258 (5), 6.5711 (2), 12.7688 (4)	25.6082 (11), 6.8565 (3), 13.4709 (8)	35.010 (3), 4.6438 (3), 13.5997 (8)
β (°)	108.450 (4)	96.374 (3)	104.060 (5)	94.795 (7)
V (Å³)	2163.93 (16)	1094.51 (6)	2294.4 (2)	2203.3 (3)
Z	8	4	8	8
Radiation type	Mo $K\alpha$	Mo $K\alpha$	Mo $K\alpha$	Mo $K\alpha$
μ (mm⁻¹)	0.11	0.11	0.11	0.10
Crystal size (mm)	$0.12\times0.06\times0.04$	$0.14\times0.06\times0.05$	$0.14\times0.12\times0.07$	$0.08\times0.05\times0.01$
Data collection				
– Diffractometer: Rigaku FRE+ equipped with HF Varimax confocal mirrors and an AFC12 goniometer and HG Saturn 724+ detector diffractometer				
– Absorption correction: Multi-scan *CrysAlis PRO* 1.171.39.9g (Rigaku Oxford Diffraction, 2015) Empirical absorption correction using spherical harmonics, implemented in SCALE3 ABSPACK scaling algorithm				
T_{min}, T_{max}	0.804, 1.000	0.658, 1.000	0.910, 1.000	0.731, 1.000
No. of measured, independent and observed [$I > 2\sigma(I)$] reflections	9681, 2481, 2023	9755, 2493, 1938	9872, 2627, 2242	15178, 2511, 2272
R_{int}	0.029	0.036	0.024	0.047
$(\sin\theta/\lambda)_{max}$ (Å⁻¹)	0.649	0.649	0.649	0.649
Refinement				
$R[F^2 > 2\sigma(F^2)]$, $wR(F^2)$, S	0.043, 0.110, 1.05	0.045, 0.106, 1.03	0.039, 0.109, 1.07	0.076, 0.195, 1.19
No. of reflections	2481	2493	2627	2511
No. of parameters	156	156	165	156
H-atom treatment	H-atom parameters constrained	H-atom parameters constrained	H-atom parameters constrained	H-atom parameters constrained
$\Delta\rho_{max}$, $\Delta\rho_{min}$ (e Å⁻³)	0.34, −0.27	0.34, −0.26	0.43, −0.19	0.68, −0.30
CCDC no.	1573020	1573018	1573019	1573021

Computer programs: *CrysAlis PRO* 1.171.39.9g [42]; SHELXT [43]; ShelXle [44] *SHELXL2014*/17, *SHELXL7* [45]; *Mercury* [46]; *PLATON* [47].

grid. Relaxed energy profiles were generated for rotation of the C(O) OCH$_2$CH$_3$ chain for forms Aa and Ca of coumarin **2d** by optimizing the molecule at fixed torsion angle values with step sizes of 10°.

Results and discussion

The colourless compounds, **2a–2d**, crystallize in *monoclinic* phases: compounds **2a**, **2b** and **2d** in the *C*2/*c* with Z = 8 and compound **2c** in the *P*2$_1$/*c* with Z = 4. The asymmetric unit in each case was a single molecule. The atom arrangements and numbering schemes are illustrated in Figure 2.

Molecular conformations of 2a–2d

The coumarin cores are very near planar in each of the four compounds: in compound **2a**, ring atom outliers from the best planes are C4A [at 0.023(1)] and C3 [at −0.015(1)], with the exocyclic carbonyl atom, O2, −0.039(1) Å out of the best plane; in compound **2b**, ring atom outliers from the best planes are C3 [at 0.087(1) Å] and O1 [at 0.064(1) Å], with the exocyclic carbonyl atom, O2 −0.061(1) Å out of the best

plane; in compound **2c**, ring atom outliers from the best planes are C3 [at 0.014(2) Å] and C2 [at −0.011(2) Å], with the exocyclic carbonyl atom, O2 −0.034(1) Å out of the best plane; and in compound **2d**, ring atom outliers from the best planes are C2 [at 0.010(1) Å] and O1 [at −0.020(1) Å], with the exocyclic carbonyl atom, O2 0.022(1) Å out of the best plane.

Selected bond lengths and angles are displayed in Table 2. As shown in Table 2, the C–C bond lengths in the pyran-2-one ring vary between 1.354(2) and 1.473(2) Å. Thus despite each carbon atom in the ring being formally sp^2 hydridiZed with the sixth atom in the ring an oxygen atom, there is not complete π electron delocalization within the pyran-2-one ring.

As shown by the torsion angles and the O2–O31 distances, listed in Table 2, there are differences in the molecular conformations, for example, the values of the C2–C3–C31–O31 torsion are 170.28(12), −146.89(13) and −8.2(3) are 174.979(10)°, and the d(O2–O31) distances are 2.8255(16), 2.9278(16), 4.226(2) and 2.8328(14) Å, respectively for **2a–2d**. The molecular conformation of compounds **2a** and **2d**, as judged by the shorter d(O2–O31) distances, will be termed a *s-cis* conformation, and that of **2c** will be termed, due to the longer d(O2–O31) distance, a *s-trans* conformation, see also
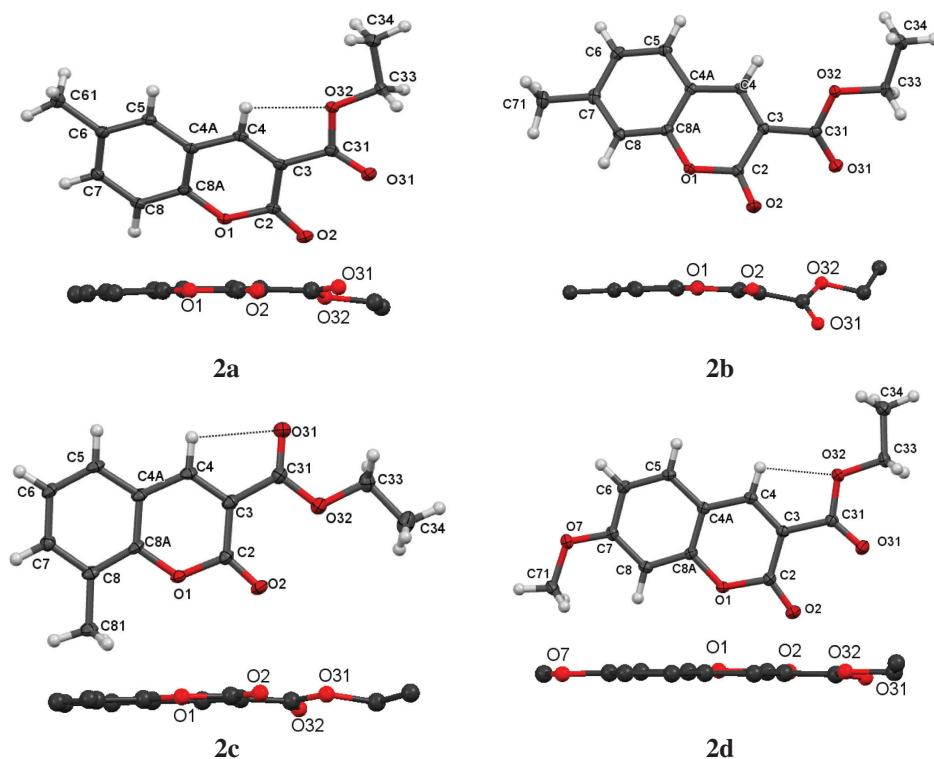

Fig. 2: Atom arrangements and side-on views of the molecular conformations of **2a–2d**. Probability ellipsoids have been drawn at the 50% level. Intramolecular hydrogen bonds have been drawn as thin dashed lines.

Tab. 2: Selected torsion angles (°) and distances, Å, in compounds, **2a–2d**.

Angle/distance	2a	2b	2c	2d
C2–O2	1.2040(17)	1.2002(18)	1.204(3)	1.2056(15)
C2–C3	1.473(2)	1.4697(19)	1.462(3)	1.4671(16)
C3–C4	1.355(2)	1.354(2)	1.356(3)	1.3615(15)
C4–C4A	1.4342(19)	1.434(2)	1.430(3)	1.4313(15)
C4A–C8A	1.398(2)	1.3965(19)	1.394(30	1.3954(16)
C8A–O1	1.3777(17)	1.3908(19)	1.372(3)	1.3761(14)
O1–C2	1.3865(16)	1.3908(17)	1.384(3)	1.4019(15)
C3–C31	1.4905(19)	1.490(2)	1.497(3)	1.4951(15)
C31–O31	1.2102(19)	1.2050(18)	1.213(3)	1.2069(15)
C31–O32	1.3436(17)	1.3389(17)	1.333(3)	1.3386(14)
O32–C33	1.4510(16)	1.4615(19)	1.457(3)	1.4580(14)
C33–C34	1.506(2)	1.505(2)	1.506(4)	1.516(17)
O31–O2	2.8255(16)	2.9278(16)	4.226(2)	2.8328(14)
O31–C31–C3–C2	−9.2(2)	36.0(2)	172.0(2)	−4.89(18)
O32–C31–C3–C2	170.28(12)	−146.89(13)	−8.2(3)	174.97(10)
C31–O32–C33–C34	−178.26(11)	−178.07(12)	−179.7(2)	173.73(10)
C4–C3–C31–O32	−6.54(18)	36.89(19)	173.8(2)	−5.93(15)
C4–C3–C31–O31	174.00(14)	−140.20(15)	−6.1(3)	174.22(12)
Interplanar angles between the coumarin core and the EtO(O) side chain	10.41(6)	36.65(6)	10.4(2)	5.64(6)

Figure 2. The molecular conformation of **2b** is somewhat in between the *s-cis* and s-*trans* conformations, from both the torsional angles and the d(O2–O31) distance, but is clearly much closer to the *s-cis* form.

Theoretical study of the molecular conformations in compounds 2a–2d

To further investigate the *s-cis* and *s-trans* molecular conformations, calculations were carried out at the M06-2X/6-31+G(d)* and M06-2X/aug-cc-pVTZ levels in implicit methanol solution [50–52]. Methanol was chosen as it was the solvent used for the recrystallizations. All possible conformations of the side chains have been considered and have been grouped in different categories, based on the extent of the rotations involving the C(O)OEt group, and additionally in **2d** that of the OMe group. Figures and energies for the most stable conformations are shown in Figure 3, with the more energetic conformations are also shown in the Supplementary Figure 1. For compounds **2a–2d**, the A and C forms (*s-cis* forms) and B and D forms (*s-trans*-forms), respectively, have the $_{\text{(coumarin)}}C(=O)–C_{\text{(OEt)}}$ fragment coplanar with its attached 2*H*-chromen-2-one unit, see Figure 3. There are only small energy differences between the A–D forms, but, of interest, **2a** has the A form, whilst compound **2b** has the B form. It is apparent that crystal packing effects result in compound **2c** being distorted from an ideal *cis* form. With consideration also of additional rotational changes involving the methoxy
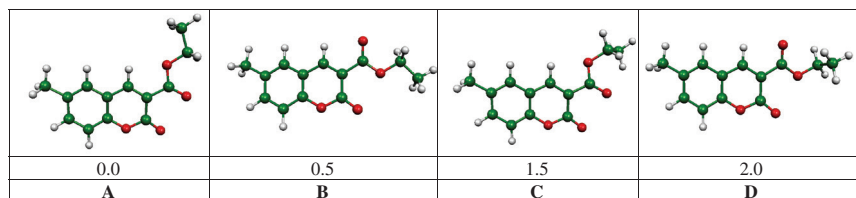
group in **2d** there are more conformations to consider. Variation of the methyl group about the coumarin unit does lead to stability differences (compare Xa and Xb structures: X = A, B, etc). However, the most stable arrangement for **2d** is calculated to be the *s-cis* form, Aa, though the *s-trans* form, Ba, is nearly iso-energetic. Of interest, the solid state experimental form of 2d matches exactly that of the theoretical solution-phase form.

Figure 4 shows the variation in conformer stability on rotating the $_{\text{(coumarin)}}C–O_{\text{(OEt)}}$ unit out of the plane of the 2d coumarin core for the Aa and Ca forms. The profiles pass through the Ba and Da forms, respectively (Aa and Ca are located near 0° Ba and Da near 180°, in the profiles). The differences between the Aa and Ca pair and between the Ba and Da pair involve rotations about the O–CH$_2$ bond of the ethyl group. As shown in Figure 4, rotations in the case of Aa and Ca from 0⁰, and in the case for Ba and Da, from 180°, result in higher energies. Overall the most stable arrangements are Aa and Ba, in which the ethyl group is fully extended.
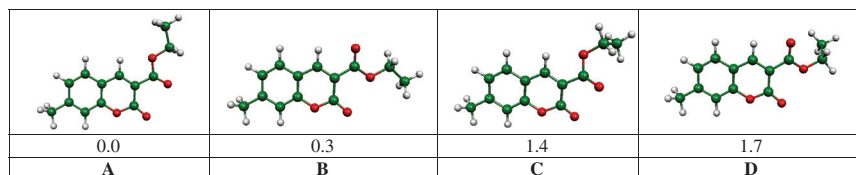
Intermolecular interactions in 2a–2d

The intermolecular interactions in **2a–2d**, as established by both the PLATON and Hirshfeld surface analyses, are listed in Table 3. Present in all four compounds are C–H···O and π···π interactions, while compound **2a** also exhibits a C=O···π interaction. Table 4 lists the contributions of various contacts, selected by the partial
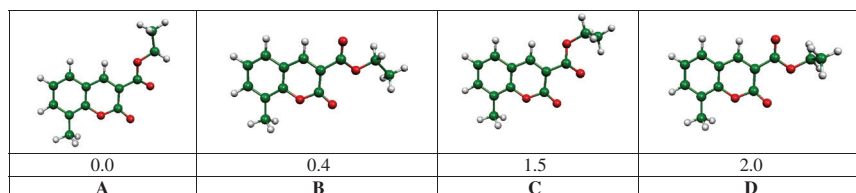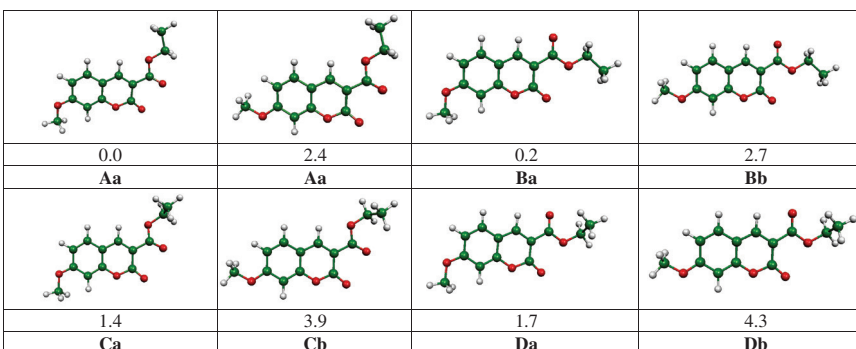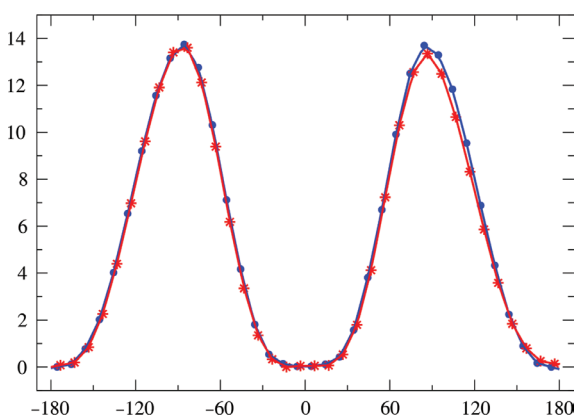
(a) Compound 2a

0.0	0.5	1.5	2.0
A	B	C	D

(b) Compound 2b

0.0	0.3	1.4	1.7
A	B	C	D

(c) Compound 2c

0.0	0.4	1.5	2.0
A	B	C	D

(c) Compound 2d

0.0	2.4	0.2	2.7
Aa	Aa	Ba	Bb

1.4	3.9	1.7	4.3
Ca	Cb	Da	Db

Fig. 3: Relative energies (kJ/mol) of the conformations, A–D, calculated at the M06-2X/aug-cc-pVTZ for compounds **2**.

Fig. 4: Variation of energy, kJ/mol^{-1}, of conformations on angle of rotation of the ester side chain about the coumarin core: minima for A and C scans occur at 0° and for B and D at 180°.

analysis of the FP plots. Some conclusions from Table 4 for the three isomers, **2a–2c** are (i) **2b** has the highest combined percentages of $O \cdots H/H \cdots O$ and $H \cdots C/C \cdots H$ interactions, but the lowest percentage of $H \cdots H$ contacts and (ii) **2c** has the highest percentage of $C \cdots C$ contacts of the three isomers. Comparison of the two compounds, **2c** and **2d**, both with substituents in the **7**-position, indicates that the most significant differences are with the $H \cdots C/C \cdots H$ and $C \cdots C$ contacts.

Although each compound has its own set of intermolecular interactions, some common, albeit superficial, features are apparent. These are (i) chain formations utilizing at least the O2 oxygen atom and (ii) sub-structures involving $\pi \cdots \pi$ interactions. These will be discussed below.

Tab. 3: Geometric parameters and symmetry operations for hydrogen bonds and intermolecular interactions (Å, °).

	D–H···A	D–H	H···A	D···A	D–H···A
Intramolecular hydrogen bonds					
2a	C4–H4···O32	0.95	2.30	2.6559(16)	101
2c	C4–H4···O2	0.95	2.45	2.772(3)	100
2d	C4–H4···O32	0.95	2.31	2.6645(13)	101

	D–H···A	D–H	H···A	D···A	D–H···A	Symmetry code
Intermolecular hydrogen bonds						
2a	C4–H4···O2	0.95	2.54	3.3973(17)	150	$1/2+x, 1-y, z$
2a	C8–H8···O31	0.95	2.51	3.4520(18)	171	$-x, -1/2+y, 1/2-z$
2a	C5–H5···O1	0.95	2.64	3.570(2)	168	$1/2+x, 1-y, z$
2b	C4–H4···O2	0.95	2.48	3.3951(17)	161	$x, 1+y, z$
2b	C71–H71C···O32	0.98	2.59	3.555(2)	170	$1-x, 1-y, 1-z$
2b	C5–H5···O1	0.95	2.50	3.200(3)	149	$x, 1+y, z$
2c	C5–H5···O2	0.95	2.50	3.200(3)	131	$x, 1-y, 1/2+z$
2c	C33–H33B···O31	0.99	2.55	3.510(3)	164	$1-x, y, 1/2-z$
2d	C4–H4···O2	0.95	2.54	3.4506(14)	161	$x, -1+y, z$
2d	C34–H34B···O31	0.98	2.48	3.2613(16)	136	$x, -1+y, z$
2d	C5–H5···O1	0.95	2.61	3.599(14)	127	$x, -1+y, z$

	Y–X···Cg	X···Cg	X_{perp}	γ	Y–X···Cg	Y···Cg
Y–X···π interactions						
2a	C2–O2···Cg2^i	3.9028(12)	3.859	8.65	109.78(9)	4.4567(15)

Symmetry codes: $i = -x, -1/2+y, 1/2-z$.

	CgI···Cg(J)	Cg···Cg	α	β	γ	CgI_{perp}	CgJ_{perp}	Slippage
π···π interactions[a]								
2a	Cg1···Cg1^i	3.9829(8)	0.02(6)	32.9	32.9	3.3441(5)	3.3441(5)	2.163
2a	Cg1···Cg2^i	3.5446(8)	1.59(6)	21.0	19.8	3.3360(5)	3.3100(6)	1.268
2a	Cg2···Cg1^i	3.5446(8)	1.59(6)	19.8	21.0	3.3100(6)	3.3360(5)	1.198
2b	Cg2···Cg1^{ii}	4.0944(8)	15.47(7)	45.1	29.8	3.5518(6)	2.8897(6)	2.901
2b	Cg1···Cg2^{iii}	4.0944(8)	15.47(7)	29.8	45.1	2.8897(6)	3.5518(6)	2.037
2b	Cg1···Cg2^{iv}	3.7243(8)	4.36(7)	27.3	26.0	3.3475(6)	3.3081(6)	1.711
2b	Cg2···Cg1^{iv}	3.7243(8)	4.36(7)	26.0	27.3	3.3082(6)	3.3474(6)	1.632
2b	Cg2···Cg2^{iv}	3.6368(8)	0.00(7)	25.4	25.4	3.2841(6)	3.2840(6)	1.563
2c	Cg1···Cg2^v	3.4454(13)	0.70(10)	17.6	18.1	3.2756(9)	3.2848(9)	1.039
2c	Cg2···Cg1^{vi}	3.4454(13)	0.70(10)	18.1	17.6	3.2849(9)	3.2757(9)	1.068
2d	Cg1···Cg1^{vii}	3.5356(7)	6.79(5)	17.4	17.4	3.3733(4)	3.3733(4)	1.059
2d	Cg1···Cg2^{vii}	3.6713(7)	7.16(5)	26.8	23.1	3.3770(4)	3.2770(5)	1.655
2d	Cg2···Cg1^{vii}	3.6714(7)	7.16(5)	23.1	26.8	3.2771(5)	3.3770(4)	1.440
2d	Cg2···Cg1^{iv}	3.4748(7)	3.7014(7)	20.1	20.1	3.2631(5)	3.2625(4)	1.196
2d	Cg2···Cg2^{iv}	3.7014(7)	0.03(5)	27.9	27.9	3.2721(5)	3.2722(5)	1.730
2d	Cg1···Cg1^{iv}	3.4750(7)	0.89(5)	20.1	20.1	3.2625(4)	3.2632(5)	1.194

[a]α, Dihedral angle between planes I and J (°); β, angle Cg(I)→Cg(J); γ, angle Cg(I)→Cg(J) vector and normal to plane J (°); Cg–Cg, distance between ring centroids (Å); CgI_{perp}, perpendicular distance of Cg(I) on ring J (Å); CgJ_{perp}, perpendicular distance of Cg(J) on ring I (Å). Symmetry codes: $i = 1/2-x, 1/2-y, 1/2-z$; $ii = 1-x, 1/2+y, 3/2-z$, $iii = 1-x, -1/2+y, 3/2-z$; $iv = 1-x, 1-y, 1-z$; $v = x, -1+y, z$; $vi = x, 1+y, z$; $vii = 1-x, y, 1/2-z$.

Tab. 4: Percentages for the most relevant atom–atom contacts for the studied compounds (%).

	H···H	H···O/O···H	H···C/C···H	C···C	C···O/O···C	O···O
2a	40.3	31.0	15.7	6.2	5.0	1.8
2b	37.9	36.8	16.9	6.0	2.1	0.4
2c	43.9	30.2	13.7	7.9	3.3	1.1
2d	39.6	36.9	6.8	11.2	4.0	1.6

Chain formation utilizing C−H−O hydrogen bonds, utilizing the carbonyl O2 oxygen

In each of the four compounds, chains of molecules are formed from C−H···O hydrogen bonds, utilizing, at least, the O2(carbonyl oxygen) atom. In **2a** and **2b**, the molecular chains are generated from C4−H4···O2 and C5−H5···O1(pyran) hydrogen bonds, thereby providing C5,C5, $R_2^2(8)$ chains [55], while in compound **2d**, additional C34−H34B···O31(ester) hydrogen bonds result in a more complex C5,C5,C6, $R_2^2(8)$ $R_2^2(13)$ arrangement [55], see Figure 5. The zig-zag chains in

(a)

(b)

(c)

(d)
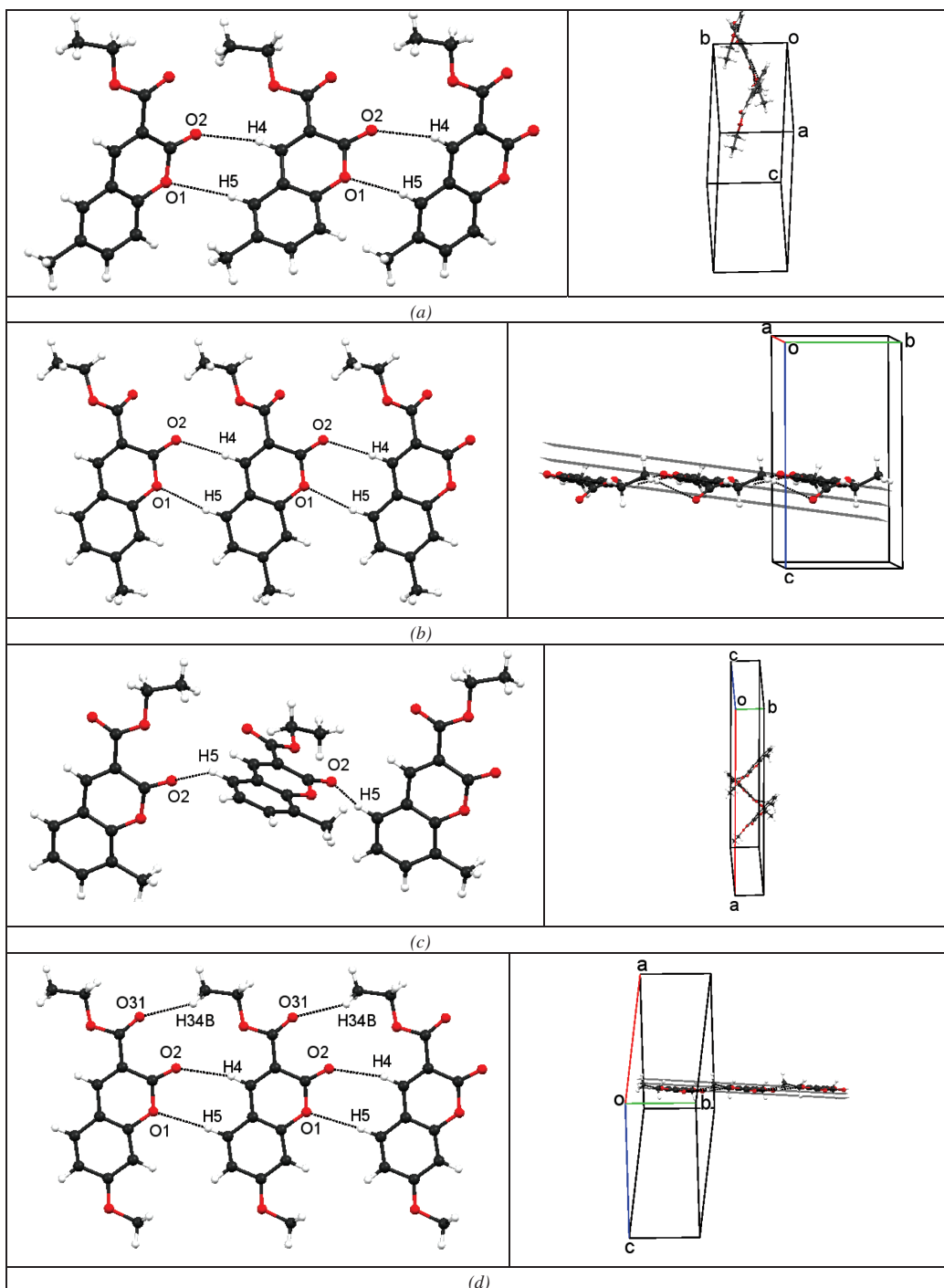
Fig. 5: Two views of the molecular chains in (a) **2a**, (b) **2b**, (c) **2c** and (d) **2d**. Intermolecular interactions are drawn as dashed lines. Table 3 lists the symmetry codes for the intermolecular interactions.

2a are propagated in the direction of the *c* axis, while in **2b** and **2d**, the chains are propagated in the direction of the *b* axis, with the coumarin cores in adjacent molecules parallel but separated by perpendicular distances of 0.86 and 0.42 Å, respectively in **2b** and **2d**, see Figure 5b and d.

In compound **2c**, the chains, C7, of molecules are obtained solely from C5–H5B···O2 hydrogen bonds and are thus very different from the chains in **2a**, **2b** and **2d**. The absence of C4–H4···O2 and C5–H5···O1 hydrogen bonds in **2c** follows from the large H4–O2 and H5B–O1 distances of 2.834 and 4.428 Å, respectively. Successive molecules in the chain are near orthogonal, with an interplanar angle of 89.91°, see Figure 5c.

It is argued that if **2c** produced a similar chain to those found in **2b** and **2d**, it would result in severe steric hindrance between the C8-methyl group and to a C61-hydrogen in an adjacent molecule. The shortest C8···H61 separations are 2.814 and 2.873 Å, respectively in **2b** and **2d**. However, the reverse situation with Me on C61 and H8 on C8, does not prevent chain formation in compound **2a**: the H8–H61C distance in **1** is 2.655 Å. Interestingly, the O1 ring oxygen is not utilized in any intermolecular interaction in **2c**. The lack of C4–H4vO32 hydrogen bonds in **2b** apparently arises from the larger rotation of the C(O)OEt group out of the coumarin plane, which results in a too long H4–O32 distance [>2.70 Å] for C4–H4···O32 hydrogen bonding.
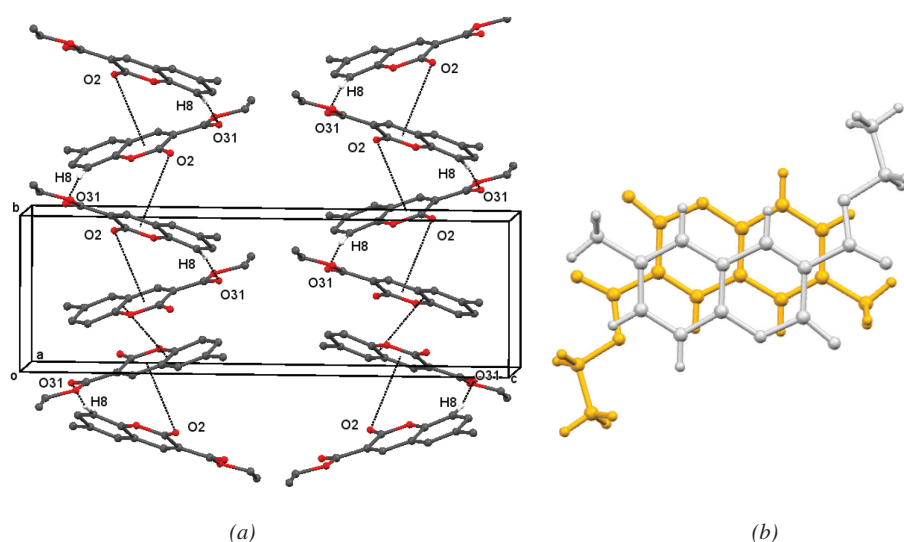
Other intermolecular interactions

Compound 2a

Other intermolecular interactions present in **2a** are C8–H8···O31 hydrogen bonds, C=O···π and π···π interactions, see Table 4. The combinations of these additional interactions generate chains, two of which pass though the unit cell, as shown in Figure 6a. The overlap of the π systems in the chain, shown in Figure 6b, involves both rings and with a perpendicular distance of 3.317 Å between parallel coumarin cores, this is clearly an important interaction. The Hirshfeld surfaces for **2a** are shown in Supplementary Figure 2.

Compound 2b

As well as the C4–H4···O2 and C5–H5···O1 hydrogen bonds, other intermolecular interactions identified in **2b** are a C71–H71C···O32 hydrogen bond and π···π interactions, see Table 3 and Figure 7. There are two distinct π···π stacking interactions, which generate chains, see Figure 7. The stronger of the two π···π interactions, π···π^i, is augmented by C71–H71C···O32^i hydrogen bonds; and has a Cg(coumarin)–Cg(coumarin) separation of 3.6368(8) Å, and a strong overlap of the π systems, see Figure 7 [i = 1 − x, 1 − y, 1 − z]. The second

(a)   *(b)*

Fig. 6: Compound **2a**. (a) Parts of two single molecular-wide chains of molecules, passing through the unit cell, derived from combinations of C8–H8···O31 hydrogen bonds, C=O···π(pyran) and π(coumarin)···π(coumarin) interactions, (b) the view of the overlap of the interacting π systems in the π···π interactions. Intermolecular interactions are drawn as dashed lines. Table 3 lists the symmetry codes for the intermolecular interactions.
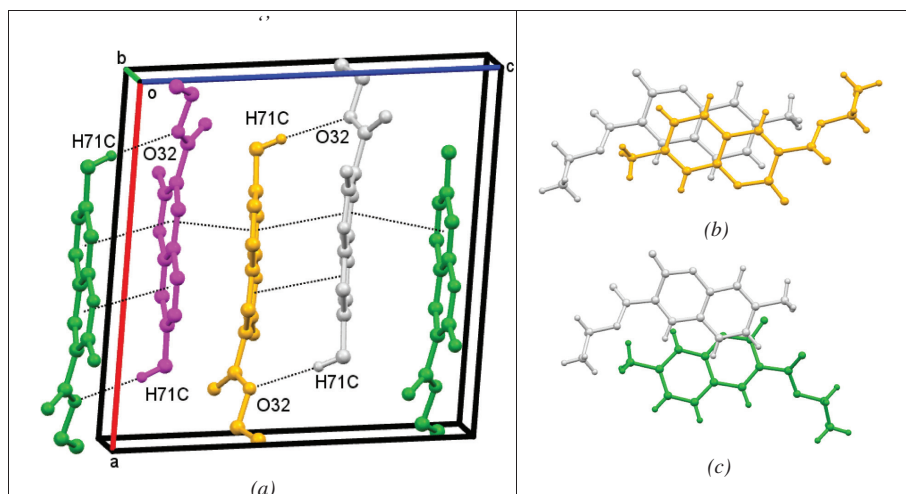
Fig. 7: Compound **2b**. (a) Part of the column of molecules, coloured according to symmetry codes, generated from combinations of C71–H71C–O32 hydrogen bonds, and $\pi\cdots\pi^{\mathrm{i}}$ and $\pi\cdots-\pi^{\mathrm{ii}}$ interactions: symmetry codes: i = 1 − x, 1 − y, 1 − z; ii = 1 − x, −1/2 + y, 3/2 − z, (b) and (c) illustrates the π overlaps in the $\pi\cdots\pi$ stacks shown in Figure 7a. Intermolecular interactions are drawn as dashed lines. Table 3 lists the symmetry codes for the intermolecular interactions.

interaction, $\pi\cdots\pi^{\mathrm{ii}}$, has a much reduced π overlap, with a longer Cg–Cg separation of 4.0944(8) Å, see Figure 7b and c: symmetry operation: ii = 1 − x, −1/2 + y, 3/2 − z. As reported earlier, the EtOC(O) unit is out of the plane of its attached coumarin core. A consequence of this is that the distance between H71C and O32$^{\mathrm{i}}$ is sufficiently short to allow the formation of C71–H71C $\cdots$ O32 hydrogen bonds. The Hirshfeld surface for **2b** is shown in Supplementary Figure 3.

Compound 2c

The additional intermolecular interactions in **2c** are C33–H33B $\cdots$ O31 hydrogen bonds and $\pi\cdots\pi$ interactions, which combine to form the chevron-shaped sub-structure, shown in Figure 8a and b. The arrangement can be considered as being made up from symmetric dimers, formed from pairs of C33–H33B $\cdots$ O31 hydrogen bonds, which are then linked via $\pi\cdots\pi$ interactions into the chevron array.
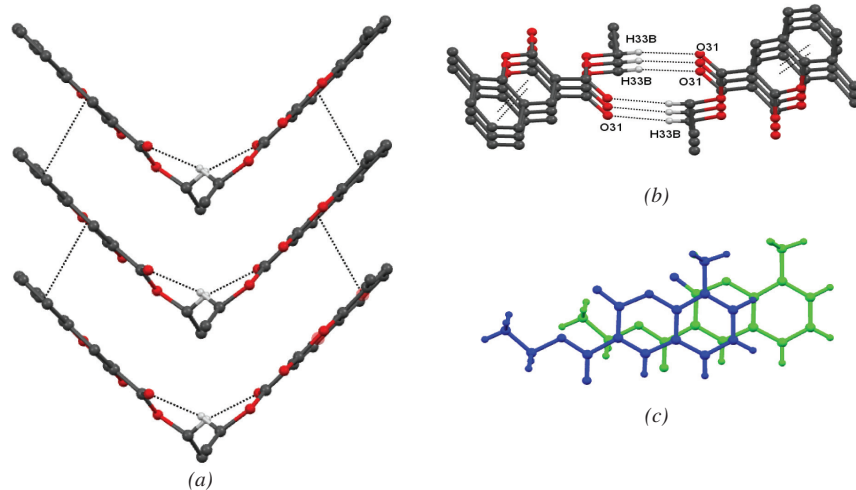
Fig. 8: Compound **2c**. (a) and (b) Two views of the chevron-type arrangement of molecules generated from C33–H33B $\cdots$ O31 hydrogen bonds and $\pi\cdots\pi$ interactions: within this arrangement are $R^2_2(10)$ rings, better seen in Figure 8b, (c) the overlap of the π systems in the $\pi\cdots\pi$ stacks. Intermolecular interactions are drawn as dashed lines. Table 3 lists the symmetry codes for the intermolecular interactions.

The angle between the coumarin units in the chevron is near orthogonal, at 89.79°. The overlap of the π systems is extensive as shown in Figure 8c, and with a perpendicular distance between the parallel coumarin units in the $\pi \cdots \pi$ stack of only 3.281 Å – this interaction appears a critical one.

The Hirshfeld surface for **2c** is shown in Supplementary Figure 4.

Compound 2d

The additional intermolecular interactions in **2d** are two distinct $\pi \cdots \pi$ interactions, $\pi \cdots \pi^i$ and $\pi \cdots \pi^{ii}$, which alternate to form stacks of molecules: symmetry codes: $i = 1 - x$, y, $1/2 - z$ and $ii = 1 - x$, $1 - y$, $1 - z$, see Figure 9a. The orientation of the molecules alternates in successive rows of the stack. The distance between the best planes through parallel coumarin cores in the $\pi \cdots \pi^{ii}$ interactions is 3.2721(5) Å. Due to the coumarin cores in the $\pi \cdots \pi^i$ interaction not being parallel, the equivalent distance varies between 3.27 and 3.37 Å, with good overlaps of the π systems, see Figure 9b and c. Thus, both $\pi \cdots \pi$ interactions appear important interactions. These $\pi \cdots \pi$ stacks are linked primarily by the three C–H$\cdots$O hydrogen bonds, namely C4–H4$\cdots$O2, C5–H5$\cdots$O1 and C34–H34B$\cdots$O31 hydrogen bonds, shown in Figure 5d, into a three dimensional array. In addition there is the possibility of further support from a weak C34–H34A$\cdots$O7^i hydrogen bond, with parameters d(H34A–O7) = 2.62 Å, C34–H34A$\cdots$O7 angle = 163° and symmetry code: $i = \frac{1}{2} + x$, $\frac{1}{2} - y$, $\frac{1}{2} + z$.

The Hirshfeld surface for **2d** is shown in Supplementary Figure 5.

Finger print (FP) plots

The FP plots for all compounds, shown in Figure 10, exhibit two pairs of spikes pointing south-west (d_e, d_i) ≅ (1.4, 1.0) Å, corresponding to H$\cdots$O close contacts and a light blue area spread around $d_e \cong d_i \cong 1.8$ Å that is due to C$\cdots$C close contacts. The areas with higher intensity of pixels spread around $d_e \cong d_i \cong 1.6$ Å are due to H$\cdots$H contacts. Of the three isomers, compounds **2a–2c**, **2b** has the highest percentage sum of all oxygen close contacts, and **2c** the highest percentages of H$\cdots$H contacts. Compound, **2d**, with the additional oxygen atom, has the highest percentage sum of all oxygen contacts, the highest percentage of C$\cdots$C contacts and the lowest percentage of C$\cdots$H/H$\cdots$C contacts, of all four compounds. Compound **2d** has a higher percentage of C$\cdots$C and C$\cdots$H/H$\cdots$C contacts than does **2b**, see the light blue area spread around $d_e \cong d_i \cong 1.6$ Å.

Comparisons of reported solid state molecular conformations of alkyl 2*H*-chromene-3-carboxylates

A survey of the CCDC data base for organyl 2*H*-chromene-3-carboxylates on Jun 22nd, 2017 [56] revealed 61 hits, of which *ca.* 50 compounds were unique and had sufficient deposited data to enable distances and angles to
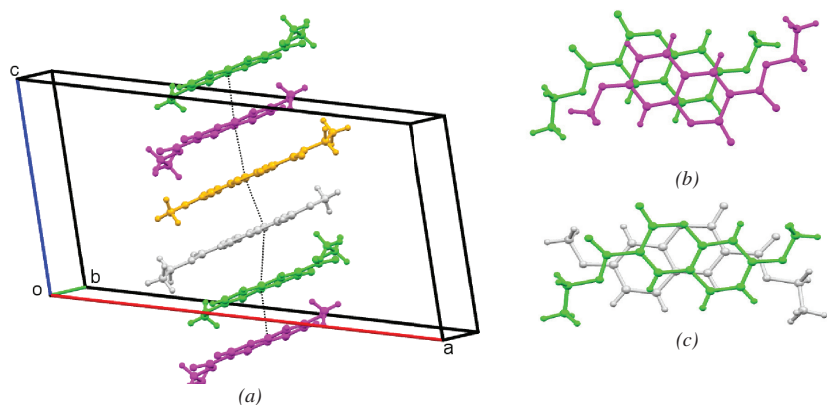
Fig. 9: Compound **2d**. (a) Part of a $\pi \cdots \pi$ stack formed from alternating, $\pi \cdots \pi^i$ and $\pi \cdots \pi^{ii}$ interactions: symmetry codes: $i = 1 - x$, y, $1/2 - z$ and $ii = 1 - x$, $1 - y$, $1 - z$; the molecules are coloured according to symmetry operations, (b) and (c) overlaps of the π systems in the $\pi \cdots \pi^i$ and $\pi \cdots \pi^{ii}$ interactions. Intermolecular interactions are drawn as dashed lines. Table 3 lists the symmetry codes for the intermolecular interactions.
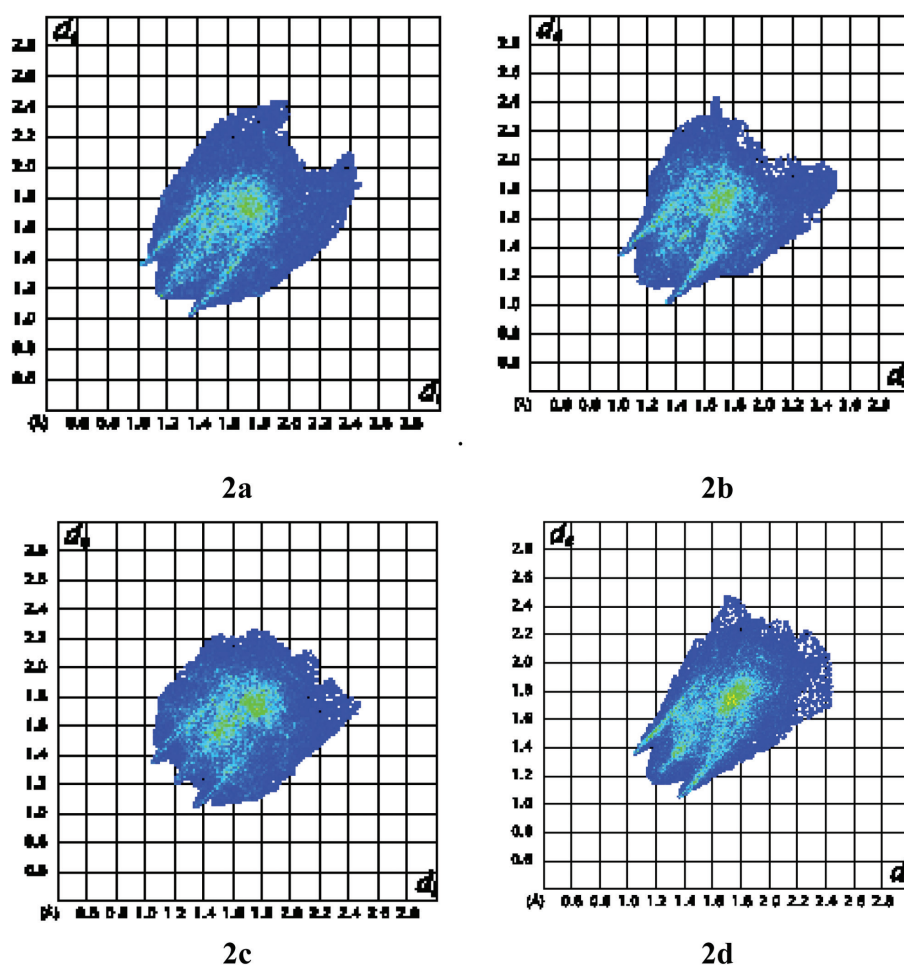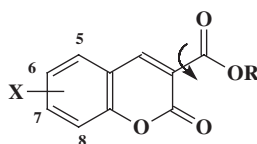
2a

2b

2c

2d

Fig. 10: The FP plots for **2a–2d**. The southwest spikes ending at $(d_e, d_i) \cong (1.4, 1.0)$ Å are present in all the plots and are due to the C–H$\cdots$O hydrogen bonds: the light blue area around $d_e \cong d_i \cong 1.8$ Å is present in all structures and indicate C$\cdots$C close contacts. The plot for compound **2d** also presents a light blue area around $d_e \cong d_i \cong 1.6$ Å, due to H$\cdots$H contacts.

be obtained. The substituents in the coumarin moiety and the carboxylate unit, both alkyl and aryl, varied greatly in terms of steric bulk and electronic effects. With the numbering scheme adopted in this study, see Figure 2, values have been obtained for the C4–C3–C31–O31 and C4–C3–C31–O32 torsion angles, interplanar angles between the coumarin core and the C3, O31, O32, C32 atoms of the carboxylate side chain and the distance between the two carbonyl oxygen atoms, O2 and O31. Aspects of these geometric parameters will be discussed here, whilst fuller details are provided in Supplementary Table 1.

Without constraints such as the intramolecular N–H(amido)$\cdots$O(carbonyl) hydrogen bonds found in the 2H-chromene-3-carboxamides [39, 40], values of the angles between the coumarin core and the carboxylate side chains vary between 0.00°, in dimethyl 4-(8-t-butyl-3-(methoxycarbonyl)-2-oxo-2H-chromen-6-yl)-

2,6-dimethyl-1,4-dihydropyridine-3,5-dicarboxylate, **2e**, (Ref. [57]: CCDC codes: GIGDOR; 877578), to 60.73°, in the $P2_1/n$ phase of ethyl 8-methoxy-2-oxo-2H-1-benzo-pyran-3-carboxylate, **2f** (Ref. [58]: CCDC codes: ADAZUB: 610860), see Figure 1. The large majority of the compounds have interplanar angles of <20°. Even in related compounds, such angles can be very different, e.g. the interplanar angle, 60.73°, in **2f**, which was recrystallised from $CHCl_3$, is very different from that of its ethoxy analogue, **2g** (Ref. [59]: CCDC codes: EYIJUT: 1447837), recrystallised from MeOH, as well as that found in its co-crystal with 2-aminobenzothiazole, (Ref. [60]: GUFDOB: 672097), values being 14.20(8) and 4.48(8)°, respectively.

It is interesting to compare the dihedral angles and O2–O31 distances in the simple alkyl 2H-chromene-3-carboxylates, having no substituent in the phenyl ring of the coumarin moiety, thereby attempting to eliminate potential steric effects of ring substituents, see Table 5a.

Tab. 5: Values of $d(O_2–O_{31})$ and the C4–C3–C31–O31 torsional angles in published organyl 2H-chromene-3-carboxylate structures.

R	C4–C3–C31–O31°	$d(O_2–O_{31})$ Å	cis or trans	CCDC codes
(a) Alkyl 2H-chromene-3-carboxylates, (X＝H)				
Me	−1.4(2)	4.243(18)	*trans*	CEHGUT: 896978
Et	−162.22(14)	2.7948(17)	*cis*	MURCUX: 1011994
i-Pr	173.72(10)	2.8433(12)	*trans*	ILICOX: 1448007
	−177.64(12)	2.8527(12)		
t-Bu	41.0(2)	4.001(16)	Close to *trans*	JELYOP: 247583
		$d(O_2–O_{31})<3.0$ Å*		$d(O_2–O_{31})>3.9$ Å

(b) All organyl 2H-chromene-3-carboxylate derivatives									
$C_4–C_3–C_{31}＝O_{31}$°	130–150	150–160	160–170	170–180	0–10	10–20	20–30	30–40	40–50
No. of molecules	5	5	11	12	11	6	5	0	2
Total				33					24

*The numbering scheme is that used in this article.

No trend in the geometric parameters with the bulk of the R group is apparent.

The designation of a *s-cis* or a *s-trans* form for each compound was primarily obtained from the O2–O31 distance: values less than 3 Å clearly have *s-cis* forms and those greater than 4 Å have *s-trans*-forms. Values of torsional angles can also be used, e.g. values of the torsional angle, C4–C3–C31–O31°, angles greater than 150° or less than 30° are clearly indicators of *s-cis* and *s-trans* forms, respectively. There are some compounds exhibiting intermediate values, e.g. 8-methoxy-2H-chromene-3-carboxylate [CCDC codes: ADAZUB: 610860] has C4–C3–C31–O31 and d(O2–O31) values of −121.89(15)° and 3.0865 Å, respectively.

The distance between the two carbonyl oxygen atoms, O2 and O31, range from 2.773(3) (Ref. [61]: CCDC codes: PUGSAM 754378) to 4.329(2) Å (Ref. [62]: CCDC codes: XOTRAB; 996298), see the Supplementary Table 2. There are two distinctly popular ranges, namely 4.094(2)–4.329(2) (*s-trans* compounds) and 2.777(3) – 3 Å (*s-cis* compounds). As shown in Table 5b, there is just a slight excess of compounds having the shorter O2–O31 distances. This is in agreement with the theoretical M06-2X/study on the simple compounds, **2a–2d**, which showed that the A and B forms, have very similar stabilities, but with a slight preference for the A form. Interestingly, in (2R,3R)-diethyl tartrate 2,3-bis(7-diethylaminocoumarin-3-carboxylate), **2h**, see Figure 1, (Ref. [63]: CCDC codes: OKIRIJ: 154949), the two carboxylate units have different orientations w.r.t. their attached coumarin moieties, with O2–O31 distances of 2.848(9) and 4.184(9) Å.

Conclusions

The theoretical and the crystallographic study of the four ethyl 2H-chromene-3-carboxylate derivatives and the survey of the published literature on organyl 2H-chromene-3-carboxylates led to the same conclusion that the favoured conformations had the ester chain near planar to the coumarin cores.

Theoretical calculations of the molecular conformations in methanol of the four ethyl 2H-chromene-3-carboxylate derivatives indicated only small differences in energies (at most <0.5 KJ/mol) between the *s-cis* and *s-trans* forms, with the *s-cis* form being the more favoured in **2a–2c** and equal stabilities for the two forms of **2d**. Rotations of the ester group out the coumarin plane resulted in a Gaussian distribution of stabilities with the maximum energy occurring at around 90°. Rotations about the C–C bond of the ester ethyl group in all four molecules and about the O–C bond of the 7-methoxyl substituent in **2d** were calculated to affect the energies as well, with extended forms leading to greater stability. The solid state molecular conformations of compounds **2a** (*s-cis* form), **2c** (*s-trans* form) and **2d** (*cis* form) were close to the calculated low energy forms: differences arose from the small interplanar angles of 10.41(6), 10.4(2) and 5.64(6)°, respectively. A greater rotation of the ester group by 36.65(6)° in **2b**, resulted in a greater difference between the experimental and calculated structures. The survey of organyl 2H-chromene-3-carboxylate compounds indicated two distinct groupings: *s-trans* compounds, with carbonyl oxygen–carbonyl distances of 4.094(2)–4.329(2) Å and

interplanar angles less than 30° and *s-cis* compounds with equivalent parameters of 2.777(3) − 3 Å and angles greater than 150°. Very few compounds had intermediate values.

The Hirshfeld surface and PLATON analysis confirmed the presence in **2a–2d** of (i) C−H⋯O hydrogen bonds, which lead primarily to molecular chains, and (ii) π⋯π interactions, which provide molecular dimers and stacks.

Supplementary material

Supplementary Figure 1 shows all the calculated conformations, A–G, for compounds **2a–2d** and their energies, Supplementary Figures 2–5 show the Hirshfeld surfaces of compounds **2a–2d**, respectively and Supplementary Table 1 lists information on conformations of 2*H*-chromene-3-carboxylate derivatives.

Full details of the crystal structure determinations in cif format are available in the online version, at https://doi.org/10.1515/zkri-2018-2117. The cif-files have also been deposited with the Cambridge Crystallographic Data Centre with deposition numbers 1573018-1573021 for compounds **2b**, **2c**, **2a** and **2d**, respectively, copies of which can be obtained free of charge on written application to CCDC, 12 Union Road, Cambridge, CB2 1EZ, UK (fax: +44 1223 336033); on request by e-mail to deposit@ccdc.cam.ac.uk or by access to http://www.ccdc.cam.ac.uk.

References

[1] M. Costa, T. A. Dias, A. Brito, F. Proenca, *Eur. J. Med. Chem*. **2016**, *123*, 487.

[2] E. C. Gaudino, S. Tagliapietra, K. Martina, G. Palmisano, G. Cravotto, *RSC Adv*. **2016**, *6*, 46394.

[3] H. Wei, J. Ruan, X. Zhanga, *RSC Adv*. **2016**, *6*, 846.

[4] B. J. Connell, S.-Y. Chang, E. Prakash, R. Yousfi, V. Mohan, W. Posch, D. Wilflingseder, C. Moog, E. N. Kodama, P. Clayette, *PLoS One* **2016**, *11*, e0165386.

[5] D. Yu, M. Suzuki, L. Xie, S. L. Morris-Natschke, K.-H. Lee, *Med. Res. Rev*. **2003**, *23*, 322.

[6] S. K. Yusufzai, H. H. Osman, M. S. Khan, S. Mohamad, O. Sulaiman, T. Parumasivam, J. A. Gansau, N. Johansah, Noviany, *Med. Chem. Res*. **2017**, *26*, 1139.

[7] G. X. Pang, C. Niu, N. Mamat, H. A. Aisa, *Bioorg. Med. Chem. Lett*. **2017**, *27*, 2674.

[8] J. Suthiwong, Y. Thongsri, C. Yenjai, *Nat. Prod. Res*. **2017**, *31*, 453.

[9] G. Kirsch, A. B. Abdelwahab, P. Chaimbault, *Molecules* **2016**, *21*, 322.

[10] V. T. Angelova, V. Valcheva, N. G. Vassilev, R. Buyukliev, G. Momekov, I. Dimitrov, L. Saso, M. Djukic, B. Shivachev, *Bioorg. Med. Chem. Lett*. **2017**, *27*, 223.

[11] R. S. Keni, B. S. Sasidhar, B. M. Nagaraja, M. A. Santos, *Eur. J. Med. Chem*. **2015**, *100*, 257.

[12] S. Vazquez-Rodriguez, R. F. Guíñez, M. J. Matos, C. Olea-Azar, J. D. Maya, E. Uriarte, L. Santana, *Med. Chem*. **2016**, *12*, 537.

[13] R. Pingaew, A. Saekee, P. Mandi, C. Nantasenamat, S. Prachayasittikul, S. Ruchirawa, V. Prachayasittikul, *Eur. J. Med. Chem*. **2014**, *85*, 65.

[14] P. Jithin Raj, D. Bahulayan, *Tetrahedron Lett*. **2017**, *58*, 2122.

[15] A. Skoczynska, M. Małecka, M. Cieslak, J. Kazmierczak-Baranska, K. Krolewska-Golinska, A. Leniart, E. Budzisz, *Polyhedron* **2017**, *127*, 307.

[16] J. Dandriyal, R. Singla, M. Kumar, V. Jaitak, *Eur. J. Med. Chem*. **2016**, *119*, 141.

[17] G. E. Escudero, C. H. Laino, G. A. Echeverría, O. E. Piro, N. Martini, A. N. Rodríguez, J. J. M. Medina, L. L. Tévez, E. G. Ferrer, P. A. M. Williams, *Chem. Bio. Interactions* **2016**, *249*, 46.

[18] A. Montagut-Romans, M. Boulven, M. Jacolot, S. MoebsSanchez, C. Hascoët, A. Hammed, S. Besse, M. Lemaire, E. Benoit, V. Lattard, F. Popowycz, *Bioorg. Med. Chem. Lett*. **2017**, *27*, 1598.

[19] G. Wang, J. Wang, D. He, X. Li, J. Li, Z. Peng, *Chem. Bio. Drug. Des*. **2017**, *89*, 456.

[20] I. Hueso-Falcón, Á. Amesty, L. Anaissi-Afonso, I. Lorenzo Castrillejo, F. Machín, A. Estévez, *Bioorg. Med. Chem. Letts*. **2017**, *27*, 484.

[21] J. Joubert, G. B. Foka, B. P. Repsold, D. W. Oliver, E. Kapp, S. F. Malan, *Eur. J. Med. Chem*. **2017**, *125*, 853.

[22] S. Hamulakova, M. Kozurkova, K. Kuca, *Curr. Org. Chem*. **2017**, *21*, 502.

[23] M. J. Matos, S. Vazquez-Rodriguez, A. Fonseca, E. Uriarte, L. Santana, F. Borges, *Curr. Org. Chem*. **2017**, *21*, 311.

[24] M. J. Matos, P. Janeiro, R. M. F. Gonzalez, S. Vilar, N. P. Tatonetti, L. Santana, E. Uriarte, F. Borges, J. A. Fontenla, D. Vina, *Future Med. Chem*. **2014**, *6*, 371.

[25] S. R. Trenor, A. R. Shultz, B. J. Love, T. E. Long, *Chem. Rev*. **2004**, *104*, 3059.

[26] Ş. N. K. Elmas, F. Ozen, K. Koran, I. Yilmaz, A. O. Gorgulu, S. Erdemir, *J. Fluorescence* **2017**, *27*, 463.

[27] H. T. Srinivasa, H. N. Harishkumar, B. S. Palakshamurthy, *J. Mol. Struct*. **2017**, *1131*, 97.

[28] W. H. Perkin, *J. Chem. Soc*. **1868**, *21*, 181.

[29] H. Pechmann, C. Duisberg, *Ber. Dtsch. Chem. Ges*. **1884**, *17*, 929.

[30] E. Knoevenagel, *Ber. Dtsch. Chem. Ges*. **1904**, *37*, 4461.

[31] P.-H. E. Yao, S. Kumar, Y.-L. Liu, C.-P. E. Fang, C.-C. Liu, C.-M. Sun, *Comb. Sci*. **2017**, *19*, 271.

[32] P. Priyanka, R. K. Sharma, D. Katiyar, *Synthesis* **2016**, *48*, 2303.

[33] R. Pratap, V. J. Ram, *Tetrahedron* **2017**, *73*, 2529.

[34] L. S. da S. Pinto, M. V. N. de Souza, *Synthesis* **2017**, *49*, 2677.

[35] L. R. Gomes, J. N. Low, F. Cagide, A. Gaspar, J Reis, F. Borges, *Acta Crystallogr*. **2013**, *B69*, 294.

[36] T. C. Baddeley, L. R. Gomes, J. N. Low, J. M. S. Skakle, A. B. Turner, J. L. Wardell, G. J. R. Watson, *Z. Kristallogr*. **2017**, *232*, 317.

[37] W. T. Vellasco Junior, C. R. B. Gomes, T. R. A. Vasconcelos, J. L. Wardell, A. Otero-de-la-Roza, M. M. Jotani, E. R. T. Tiekink, *Z. Kristallogr*. **2016**, *231*, 663.

[38] L. N. F. Cardoso, T. C. M. Noguiera, C. R. Kaiser, J. L. Wardell, S. M. S. V. Wardell, M. V. N. de Souza, *Z. Kristallogr*. **2016**, *231*, 167.

[39] L. R. Gomes, J. N. Low, A. Fonseca, M. J. Matos, F. Borges, *Acta Crystallogr*. **2016**, *E72*, 926.

[40] L. R. Gomes, J. N. Low, A. Fonseca, M. J. Matos, F. Borges, *Acta Crystallogr*. **2016**, *E72*, 1121.

[41] L.-M. Song, J.-H. Gao, *Jiegou Huaxue* **2014**, *33*, 57.

[42] CrysAlis PRO 1.171.39.9g: *Rigaku Oxford Diffraction*, **2015**.

[43] G. M. Sheldrick, *Acta Crystallogr*. **2015**, *A71*, 3.

[44] C. B. Hübschle, G. M. Sheldrick, B. Dittrich, *J. Appl. Crystallogr*. **2011**, *44*, 1281.

[45] G. M. Sheldrick, Crystal structure refinement with *SHELXL7*. *Acta Crystallogr*. **2015**, *C71*, 3.

[46] Mercury, CCDC **2017**.

[47] A. L. Spek, *Acta Crystallogr*. **2009**, *D65*, 148.

[48] A. L. Rohl, M. Moret, W. Kaminsky, K. Claborn, J. J. McKinnon, B. Kahr, *Cryst. Growth Des*. **2008***, 8*, 4517.

[49] S. K. Wolff, D. I. Grimwood, J. J. McKinnon, M. J. Turner, D. Jayatilaka, M. A. Spackman, *Crystal Explorer*, The University of Western Australia, **2012**.

[50] Y. Zhao, D. G. Truhlar, *Theor. Chem. Acc*. **2008**, *120*, 215.

[51] S. Miertus, E. Scrocco, J. Tomasi, *Chem. Phys*. **1981**, *55*, 117.

[52] T. H. Dunning Jr, *J. Chem. Phys*. **1989**, *90*, 1007.

[53] R. A. Kendall, T. H. Dunning Jr, R. J. Harrison, *J Chem. Phys*. **1992**, *96*, 6796.

[54] M. J. Frisch, G. W. Trucks, H. B. Schlegel, G. E. Scuseria, M. A. Robb, J. R. Cheeseman, G. Scalmani, V. Barone, B. Mennucci, G. A. Petersson, H. Nakatsuji, M. Caricato, X. Li, H. P. Hratchian, A. F. Izmaylov, J. Bloino, G. Zheng, J. L. Sonnenberg, M. Hada, M. Ehara, K. Toyota, R. Fukuda, J. Hasegawa, M. Ishida, T. Naka-jima, Y. Honda, O. Kitao, H. Nakai, T. Vreven, J. A. Montgomery Jr., J. E. Peralta, F. Ogliaro, M. Bearpark, J. J. Heyd, E. Brothers, K. N. Kudin, V. N. Staroverov, R. Kobayashi, J. Normand, K. Raghavachari, A. Rendell, J. C. Burant, S. S. Iyengar, J. Tomasi, M. Cossi, N. Rega, J. M. Millam, M. Klene, J. E. Knox, J. B. Cross, V. Bakken, C. Adamo, J. Jaramillo, R. Gomperts, R. E. Stratmann, O. Yazyev, A. J. Austin, R. Cammi, C. Pomelli, J. W. Ochterski, R. L. Martin, K. Morokuma, V. G. Zakrzewski, G. A. Voth, P. Salvador, J. J. Dannenberg, S. Dapprich, A. D. Daniels, Ö. Farkas, J. B. Foresman, J. V. Ortiz, J. Cioslowski, D. J. Fox, Gaussian 09. Gaussian, Inc., Wallingford, CT, **2009**.

[55] J. Bernstein, R. E. Davis, L. Shimoni, N. L. Chang, *Angew. Chem. Int. Ed. Engl*. **1995**, *14*, 1555.

[56] C. R. Groom, I. J. Bruno, M. P. Lightfoot, S. C. Ward, *Acta Crystallogr*. **2016**, *B72*, 171.

[57] K. V. Sashidhara, M. Kumar, V. Khedgikar, P. Kushwaha, R. K. Modukuri, A. Kumar, J. Gautam, D. Singh, B. Sridhar, R. Trivedi, *J. Med. Chem*. **2013**, *56*, 109.

[58] H. Takahashi, H. Takechi, K. Kubo, T. Matsumoto, *Acta Crystallogr*. **2006**, *E62*, o2553.

[59] V. B. Nagaveni, S. Naveen, T. O. Shrungesh Kumar, M. N. Kumara, K. M. Mahadevan, N. K. Lokanath, *Der Pharma Chemica*. **2016**, *8*, 392.

[60] Y.-F. Sun, S.-Y. Ma, D. Zhang, X.-L. Cheng, Yi.-X Kexue, *Yu Guang Huaxue* **2008**, *26*, 393.

[61] C.-L. Xu, S.-Y. Liu, C.-X. Wang, M.-Q. Zhao, *Acta Crystallogr*. **2009**, *E65*, o2817.

[62] H. Moon, Q. P. Xuan, D. Kim, Y. Kim, J. W. Park, *Cryst. Growth Des*. **2014**, *14*, 6613.

[63] L.-C. Lo, J.-Y. Chen, C.-T. Yang, D.-S. Gu, *Chirality* **2001**, *13*, 266.

Graphical Synopsis

Ligia R. Gomes, John N. Low, Tanja van Mourik, Ligia S. da Silveira Pinto, Marcus V.N. de Souza and Jámes L. Wardell
Crystal structures, Hirsfeld surface analysis and a computational study of four ethyl 2-oxo-2*H*-chromene-3-carboxylate derivatives: a survey of organyl 2-oxo-2*H*-chromene-3-carboxylate structures

Synopsis: A study of the crystal structures and conformations of organyl ethyl 2-oxo-2*H*-chromene-3-carboxylates.